Laser and Particle Beams (2007), *25*, 567–584. Printed in the USA.

DOI: 10.1017/S0263034607000687

Multi-phase equation of state for aluminum

I.V. LOMONOSOV

Institute of Problems of Chemical Physics, Russian Academy of Science, Moscow, Russia

(Received 14 June 2007; Accepted 2 August 2007)

Abstract

Results of theoretical calculations and experimental measurements of the equation of state (EOS) at extreme conditions are discussed and applied to aluminum. It is pointed out that the available high pressure and temperature information covers a broad range of the phase diagram, but only irregularly and, as a rule, is not thermodynamically complete; its generalization can be done only in the form of a thermodynamically complete EOS. A multi-phase EOS model is presented, accounting for solid, liquid, gas, and plasma states, as well as two-phase regions of melting and evaporation. The thermodynamic properties of aluminum and its phase diagram are calculated with the use of this model. Theoretical calculations of thermodynamic properties of the solid, liquid, and plasma phases, and of the critical point, are compared with results of static and dynamic experiments. The analysis deals with thermodynamic properties of solid aluminum at $T = 0$ and 298 K from different band-structure theories, static compression experiments in diamond anvil cells, and the information obtained in isentropic-compression and shock-wave experiments. Thermodynamic data in the liquid state, resulting from traditional thermophysical measurements, "exploding wire" experiments, and evaluations of the critical point are presented. Numerous shock-wave experiments for aluminum have been done to measure shock adiabats of crystal and porous samples, release isentropes, and sound speed in shocked metal. These data are analyzed in a self-consistent manner together with all other available data at high pressure.

The model's results are shown for the principal shock adiabat, the high-pressure melting and evaporation regions and the critical point of aluminum. New experimental and theoretical data helped to improve the description of the high-pressure, high-temperature aluminum liquid. The present EOS describes with high accuracy and reliability the complete set of available information.

Keywords: Aluminum; Equation of state; High-energy-density matter

1. INTRODUCTION

Equation of state (EOS) describes fundamental thermophysical properties of matter. This information can only be obtained by using sophisticated theoretical models or from experiments (Al'tshuler, 1965; Bushman & Fortov, 1983; Eliezer *et al.*, 1986; Ross, 1985; Chisolm *et al.*, 2003). The EOS is of considerable interest for basic research and has numerous important applications (Bushman *et al.*, 1992, 1993; Fortov & Yakubov, 1999; Hoffmann *et al.*, 2002, 2005; Tahir *et al.*, 2005*b*, 2007; Temporal *et al.*, 2005), among them also inertial confinement fusion (Peng *et al.*, 2005; Danson *et al.*, 2005; Eliezer *et al.*, 2007). High intensity heavy ion beams as well as high power lasers and pulsed power discharges are developing into an important tool for EOS experiments (Danson *et al.*, 2005; Jungwirth, 2005; Hoffmann *et al.*, 2005; Ray *et al.*, 2006; Sasaki *et al.*, 2006; Desai *et al.*, 2007). States of matter characterized by high-energy-density occupy a broad region of the phase diagram, for example, hot compressed matter, strongly coupled plasmas, hot expanded liquid and quasi-ideal plasmas. Our knowledge of these states is limited, because theoretical modeling is complicated and experiments are difficult to perform.

Aluminum remains one of the most important metals for mankind, being of wide use in industry and science. Its thermodynamic properties have been investigated in numerous static and dynamic experiments and explored with the use of modern theories as well.

Nevertheless, the EOS for aluminum is still a "hot" problem in the physics of high energy densities. This fact is explained by a long–time intrigue of the structural phase transition at $\simeq 200$ GPa, inferred from the non-monotonic behavior of the shock adiabat. Other reasons are that properties of liquid aluminum at high pressures and temperatures are not well-known and multi-phase EOSs for aluminum have been developed in 1980 (Holian, 1986; Kerley, 1987; Bushman *et al.*, 1993).

Address correspondence and reprint requests to: I.V. Lomonosov, Institute of Problems of Chemical Physics, Russian Academy of Science, Prosp. Akad. Semenova 1, Moscow 142432, Russia. E.mail: ivl143@yahoo.com

Fortunately, recent progress achieved in both experimental and theoretical areas, i.e., Z-machine, diamond anvils, and quantum molecular dynamic calculations, significantly clarified these old problems. These advances motivated the present reassessment and refinement of the multi-phase EOS for aluminum.

It this work, an advanced multi-phase EOS for aluminum is presented. The thermodynamically complete, temperature EOS for metals is defined by the potential of free energy describing the elastic contribution at $T = 0$ K and the thermal contribution by atoms and electrons. The EOS provides for a correct description of phase boundaries, melting, and evaporation, as well as the effects of the first and second ionization. The atomic thermal contribution in the model is different in the solid and liquid states, while the electron thermal contribution is identical.

To construct the EOS, the following information was used at high pressure and high temperature: measurements of isothermal compressibility in diamond anvil cells, isentropic–compression experiments, data on sound velocity and liquid metal density at atmospheric pressure, isobaric–expansion measurements, data on the shock compressibility of solid and porous samples in incident and reflected shock waves, impedance measurements of shock compressibility obtained by an underground nuclear explosion, data on the isentropic expansion of shocked metals, calculations by the Thomas–Fermi model and by quantum molecular dynamics methods, numerous evaluations of the critical point.

New experimental and theoretical data helped to improve the description of the high-pressure, high-temperature aluminum liquid. The present EOS describes with high accuracy and reliability the complete set of available information.

2. EOS PROBLEM

EOS is a fundamental property of matter defining its thermodynamic characteristics in a functional form like $f(x, y, z) = 0$, where x, y, z can be, for example, volume V, pressure P, temperature T, or in the form of graphs or tables. Well-known functional for EOSs include, for instance, the Mie–Grüneisen EOS Grüneisen (1912)

$$P(V, E) = P_c(V) + \frac{\gamma(V)}{V}(E - E_c(V)), \tag{1}$$

where the index c indicates the component at $T = 0$ K; the Birch (1968) potential

$$P(V) = \frac{3}{2}B_T(\sigma^{7/3} - \sigma^{5/3})\left\{1 - \frac{3}{4}(4 - B_P)(\sigma^{2/3} - 1)\right\}, \tag{2}$$

in which $\sigma = V_0/V$, V_0—specific volume at normal conditions ($P = 1$ bar, $T = 298$ K), $B_T = -(\partial P/\partial \ln V)_T$—isothermal bulk compression modulus, $B_P = \partial B_T/\partial P$—its pressure derivative; and the Carnahan–Starling's approximation for the free energy of a system of "hard" spheres (Carnahan & Starling, 1969)

$$\frac{F_{HS}(V, T)}{NkT} = \frac{4\eta - 3\eta^2}{(1 - \eta)^2}, \tag{3}$$

where N–amount of particles, k–Boltzmann's constant, and η–packing density. One can find examples of EOSs in graphic or tabular form in compendia of shock wave data (van Thiel, 1977; Marsh, 1980; Zhernokletov *et al.*, 1996; Trunin *et al.*, 2001); these are EOSs of shock adiabats.

The current state of the problem of a theoretical description of thermodynamic properties of matter at high pressures and high temperatures is given in a set of publications (Zeldovich & Raizer, 1966; Eliezer *et al.*, 1986; Fortov & Yakubov, 1999; Bushman *et al.*, 1993; Bushman & Fortov, 1983; Ross, 1985, and references therein). In spite of the significant progress achieved in predicting EOS information accurately in solid, liquid, and plasma states with the use of the most sophisticated "ab initio" computational approaches (classic and quantum methods of self-consisted field, diagram technique, Monte-Carlo, and molecular dynamics methods), the disadvantage of these theories is their regional character (Eliezer *et al.*, 1986; Fortov & Yakubov, 1999; Bushman *et al.*, 1993; Bushman & Fortov, 1983; Ross, 1985). The range of applicability of each method is local and, rigorously speaking, no single one of them provides for a correct theoretical calculation of thermodynamic properties of matter on the whole phase plane from the cold crystal to the liquid and hot plasmas (Bushman & Fortov, 1983; Eliezer *et al.*, 1986; Fortov & Yakubov, 1999). The principal problem here is the need to account correctly for the strong collective interparticle interaction in disordered media, which presents special difficulties in the region occupied by dense, disordered, nonideal plasmas (Bushman & Fortov, 1983; Ross, 1985; Eliezer *et al.*, 1986; Fortov & Yakubov, 1999; Bushman *et al.*, 1993).

In this case, experimental data at high pressures and high temperatures are of particular significance, because they serve as reference points for theories and semi-empirical models. Data obtained with the use of dynamic methods (see Zeldovich & Raizer, 1966; Bushman *et al.*, 1993; Fortov & Yakubov, 1999; McQueen *et al.*, 1970; Avrorin *et al.*, 1990; Al'tshuler 1965; Duvall & Graham, 1977, and references therein) are of the importance from the practical point of view. Shock-wave methods permit to study a broad range of the phase diagram from the compressed hot condensed states to dense strongly coupled plasma and quasi-gas states. Detailed presentations of shock-wave methods to investigate high dynamic pressures can be found in the literature (Zeldovich & Raizer, 1966; Bushman *et al.*, 1993; Fortov & Yakubov, 1999; Avrorin *et al.*, 1990, and reviews, Al'tshuler, 1965; Duvall & Graham, 1977).

https://doi.org/10.1017/S0263034607000687 Published online by Cambridge University Press

Available experimental data on the shock compression of solid and porous metals, as well as isentropic expansion, covers nine orders of magnitude in pressure and four in density. The first published shock-wave data were obtained for metals in the megabar (1 Mbar = 100 GPa) (Walsh *et al.*, 1957) and multimegabar (Al'tshuler *et al.*, 1958*a*, 1958*b*) pressure range using explosive drivers. Higher pressures of 10 Mbar have been accessed by spherical cumulative systems (Kormer *et al.*, 1962; Al'tshuler *et al.*, 1981) and by underground nuclear explosions (Al'tshuler *et al.*, 1968; Trunin *et al.*, 1969). Maximum pressures of 400 TPa (Vladimirov *et al.*, 1984) were also reported for aluminum through the use of nuclear explosion. Note that data obtained by impedance-matching techniques require the knowledge of the EOS for a standard material. Previously a monotonic approximation of the shock adiabat of lead between the traditional region of pressures $\leq$10 Mbar to Thomas–Fermi calculations (Kalitkin & Kuzmina, 1975) was used for the standard (Al'tshuler *et al.*, 1968; Trunin *et al.*, 1969). It seems that iron, for which absolute Hugoniot measurements have been reported to pressures of 100 Mbar (Trunin *et al.*, 1992, 1993), is now the best etalon material. Figure 1 shows modern progress achieved in measurements of absolute shock compressibility with the use of traditional explosive techniques and investigations of impedance in experiments with concentrated energy fluxes like lasers and underground nuclear explosions.

The extension of the phase diagram data to greater relative volumes, in comparison with the principal Hugoniot, is achieved with shock compression of porous samples (Zeldovich & Raizer, 1966). Nevertheless, difficulties in fabricating highly porous targets and non-uniform material response of the porous sample to shock loading imposes a practical limit to the minimum density of a specimen. The method of isentropic expansion of shocked matter, depending on the magnitude of the shock pressure and, consequently, the entropy provided, produces in one experiment transitions from a hot metallic liquid shocked state, to a strongly coupled plasma, then to a two-phase liquid-gas region, and to a Boltzmann's weakly ionized plasma, and finally to a nearly ideal gas (Zeldovich & Raizer, 1966; Bushman *et al.*, 1993; Fortov & Yakubov, 1999).

The available experimental and theoretical information is shown in Figure 2 on a three-dimensional (3D), relative volume-temperature-pressure surface calculated by a semi-empirical multi-phase EOS (Bushman *et al.*, 1993). It is well illustrated that besides the shock compressibility, measurements of release isentropes of shocked materials are of especial importance. Such results traverse states in the intermediate region between the solid state and gas, occupied by a hot dense metallic liquid and strongly coupled plasma (Bushman *et al.*, 1993; Fortov & Yakubov, 1999), which is a region poorly described by theory. Experimentally studied release isentropes for copper have as initial high energy states solid, and melted, and compressed liquid metal. The range of thermodynamic parameters covered in the adiabatic expansion process for these states is extremely wide (Fig. 2), covering five orders of magnitude in pressure and two orders of magnitude in density. It extends from a highly compressed metallic liquid, characterized by a disordered arrangement of ions, and degenerate electrons, to a quasi-nonideal Boltzmann plasma and a rarefied metallic vapor. Upon expansion of the system, the degree of degeneracy of the electronic subsystem is decreased and a marked rearrangement of the energy spectrum of atoms and ions occurs. A partial recombination of the dense plasma also takes place. In the disordered

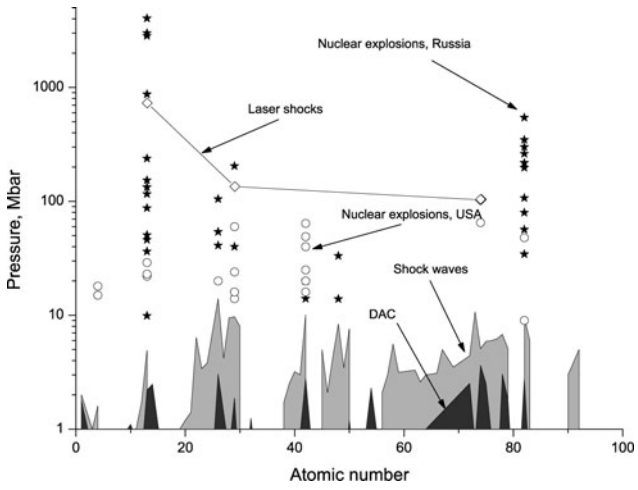

Fig. 1. The investigated pressure scale for the elements. Shown are maximum pressures achieved using traditional explosive (gray region), lasers, diamond-anvil-cell static measurements (black), and underground nuclear explosions (points).

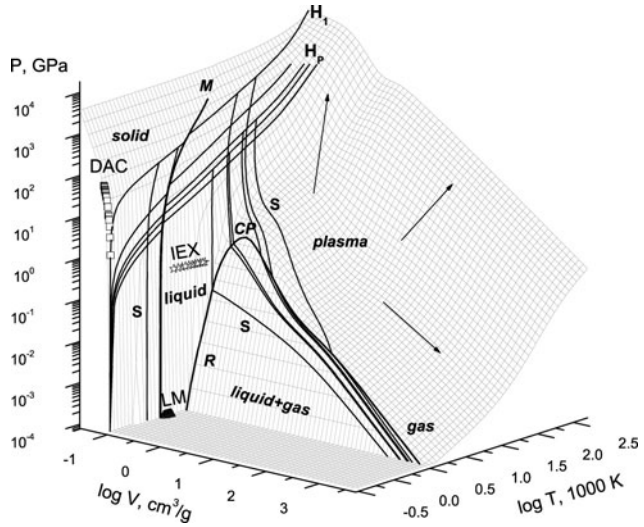

Fig. 2. Generalized 3D volume-temperature-pressure surface for copper in the investigated region of the phase diagram. M–melting region; H_1 and H_p–principal and porous Hugoniots; DAC–diamond-anvil-cells data; IEX–isobaric expansion data; S–release isentropes; R–boundary of two-phase liquid-gas region with the critical point CP. Phase states of the metal are also shown.

https://doi.org/10.1017/S0263034607000687 Published online by Cambridge University Press

electron system, a "metal-insulator" transition takes place and a nonideal (with respect to different forms of interparticle interactions) plasma is formed in the vicinity of the liquid-vapor equilibrium curve and the critical point. Where the isentropes enter the two-phase liquid-vapor region evaporation occurs; on the gas-side condensation occurs (Avrorin *et al.*, 1990; Bushman *et al.*, 1993; Fortov & Yakubov, 1999).

Note that typical shock-wave measurements allow determination of only caloric properties of matter, viz. the dependence of the relative internal energy on pressure and volume as $E = E(P, V)$. The potential $E(P, V)$ is not complete in the thermodynamic sense and a knowledge of temperature T or entropy S is required for completing the thermodynamic equations and calculating first and second derivatives, such as the heat capacity, the sound velocity and others (Fortov & Yakubov, 1999).

Only a few temperature measurements in shocked metals are available (Yoo *et al.*, 1993), as well as analogous measurements in release isentropic waves (Avrorin *et al.*, 1990). This information is of great importance in view of a limitation of purely theoretical calculation methods. From this point of view, thermodynamically complete measurements obtained with the use of the isobaric expansion (IEX) technique (Gathers, 1986) are of a special significance. In this method, metal is rapidly heated by a powerful pulsed current, then expands into an atmosphere of an inertial gas maintained at constant pressure. This data range in density form solid to the critical point and intersect, therefore, the release isentrope data for metals (see Fig. 2).

The region between principal shock adiabat and isotherm can be accessed with use of the isentropic compression technique. This method allows one to obtain simultaneously high pressure and high densities in the material under study. In practice, the sample is loaded by a magnetically driven impactor or by a sequence of reverberating shock waves in a multi-step compression process.

The final conclusion is that shock-wave techniques allow one to investigate material properties in very wide region of the phase diagram—from compressed solid to hot dense liquid, plasma, liquid-vapor, and quasi-gas states. Though the resulting high pressure, high and temperature information covers a broad range of the phase diagram, it has a heterogeneous character and, as a rule, is not complete from the thermodynamic point of view. Its generalization can be done only in the form of a thermodynamically complete EOS.

3. EOS MODEL

Wide-range EOS models for aluminum have been developed since the 1960s (see, for example, Kormer *et al.*, 1962; Holian, 1986; Kerley, 1987; Bushman *et al.*, 1992, 1993; Young & Corey, 1995). The model described below presents a modification of an existing EOS of Bushman *et al.* (1993). Changes are in the thermal electrons and the cold compression curve, which are from Bushman *et al.* (1992).

The EOS model is given by a thermodynamically complete potential of free energy F in the traditional form

$$F(V, T) = F_c(V) + F_a(V,T) + F_e(V,T), \tag{4}$$

describing the elastic contribution at $T = 0$ K (F_c), and the heat contribution by atoms (F_a) and electrons (F_e).

3.1. Elastic Curve

The elastic energy for the solid phase is given in the form of a series expansion of $r_c^{-1} \sim \sigma_c^{1/3}$ (Kormer *et al.*, 1962; Bushman *et al.*, 1992, 1993)

$$F_c^{(s)}(V) = 3V_{0c} \sum_{i=1,5} \frac{a_i}{i} (\sigma_c^{i/3} - 1), \tag{5}$$

where $\sigma_c = V_{0c}/V$, V_{0c}–specific volume at $P = 0$. Note that Eq. (5) automatically provides for the normalizing condition $F_c^{(s)}(V_{0c}) = 0$.

The conditions at $\sigma_c = 1$ for the cold pressure $P_c(V) = -dF_c(V)/dV$, bulk compression modulus $B_c(V) = -VdP_c(V)/dV$, and its pressure derivative $B_p(V) = dB_c/dP_c$ define the cold curve at moderate compressions, which together with Eq. (5) leads to the formulas

$$\sum_{i=1,5} a_i = 0, \tag{6}$$

$$\sum_{i=1,5} a_i \frac{i}{3} = B_{0c}, \tag{7}$$

$$2 + \frac{1}{B_{0c}} \sum_{i=1,5} a_i \left(\frac{i}{3}\right)^2 = B_{p0}. \tag{8}$$

Here B_{0c} and B_{p0}, together with the thermal contribution, provide for tabular values of the isentropic bulk compression modulus and its pressure derivative at normal conditions. By minimizing the mean-square deviation from the Thomas-Fermi cold pressure P_c^{TFC} (Kalitkin & Kuzmina, 1975) over N points in the interval of σ_c from 25 to 500, together with the bounding equations (6)–(8), one can define the Lagrangian problem of determining the minimum of the functional form depending on $\chi = a_i$, λ, μ, ν

$$\begin{aligned} \Upsilon(\chi) = &\sum_{n=1,N} g_n \left[1 - \frac{P_c(a_i, \sigma_n)}{P_c^{TFC}(\sigma_n)}\right]^2 \\ &+ \lambda \sum_{i=1,5} a_i + \mu \left(B_{0c} - \sum_{i=1,5} a_i \frac{i}{3}\right) \\ &+ \nu \left(B_{p0} - 2 - \frac{1}{B_{0c}} \sum_{i=1,5} a_i \left(\frac{i}{3}\right)^2\right). \end{aligned} \tag{9}$$

https://doi.org/10.1017/S0263034607000687 Published online by Cambridge University Press

Taking derivatives of Eq. (9) on a_i, λ, μ, ν one can obtain the algebraic system of eight linear equations for eight values, whose solution defines the coefficients a_i.

The cold energy for the liquid in the compression region ($\sigma_c \geq 1$) is given by Eq. (5), while in the rarefaction region ($\sigma_c < 1$) it is represented as

$$F_c^{(l)}(V) = V_{0c}\left[A_c\frac{\sigma_c^m}{m} + B_c\frac{\sigma_c^n}{n} + C_c\frac{\sigma_c^l}{l}\right] + E_{sub}. \tag{10}$$

The normalizing condition $F_c^{(l)}(\sigma_c = 0) = E_{sub}$, where E_{sub} is the tabular value of the cohesion energy, leads to the formula

$$\frac{A_c}{m} + \frac{B_n}{n} + \frac{C_c}{l} + \frac{E_{sub}}{V_{0c}} = 0. \tag{11}$$

The system of Eqs. (6)–(8) for a cold energy in the form of Eq. (10) at σ_c=1 results in

$$A_c + B_c + C_c = 0, \tag{12}$$

$$mA_c + nB_c + lC_c = B_{0c}, \tag{13}$$

$$\frac{m^2A_c + n^2B_c + l^2C_c}{B_{0c}} + 2 = B_{p0}. \tag{14}$$

Here parameter m is usually ≈ 1 (i.e., van der Waals); l is a fitting parameter, defined from the best description of the density and sound velocity data in the liquid phase. Other parameters are found from Eqs. (11)–(14).

3.2. Thermal Contribution of Atoms

The atomic thermal contribution to the free energy of the solid phase is defined by the high-temperature Debye approximation formula:

$$F_a^{(s)}(V, T) = 3RTln\frac{\theta_c^{(s)}(V)}{T}, \tag{15}$$

where R is the gas constant. The characteristic temperature $\theta_c^{(s)}$ is given by the empirical relation

$$\theta_c^{(s)}(V) = \theta_0^s\sigma^{2/3}\exp\left(\frac{(\gamma_{0s} - 2/3)(B_s^2 + D_s^2)}{B_s} \arctan\left[\frac{xB_s}{B_s^2 + D_s(x + D_s)}\right]\right), \tag{16}$$

where $x = \ln\sigma$. Constants B_s and D_s are found from the compression dependence of the Grüneisen gamma $\gamma(V) = d\ln\theta(V)/d\ln\sigma$. This information is obtained from shock-wave and isentropic–compression data in the solid state. The value of γ_{0s} is the tabulated value of the Grüneisen parameter at ambient conditions, and the normalizing condition for entropy $S(V_0, T = 293\ \mathrm{K}) = 0$ defines the value of θ_{0s}. Note that at high compression Eq. (16) provides for the correct ideal-gas asymptote $\theta_c^{(s)} \sim \sigma^{2/3}$.

The atomic thermal contribution to the free energy of the liquid phase is represented as

$$F_a^{(l)}(V, T) = F_t(V, T) + F_m(V, T). \tag{17}$$

The first term accounts for anharmonic effects and the second provides for a properly behaved melting curve.

In the liquid phase, the phonon contribution has a form similar to Eq. (16) but with a volume- and temperature-dependent heat capacity c_a and a characteristic temperature $\theta^{(l)}$:

$$F_t(V, T) = c_a(V, T)\ ln\frac{\theta^{(l)}(V, T)}{T}. \tag{18}$$

The heat capacity in the liquid phase is given by the expression

$$c_a(V, T) = \frac{3R}{2}\left[1 + \frac{\sigma T_a}{(\sigma + \sigma_a)(T + T_a)}\right], \tag{19}$$

describing a smooth variation from the value $3R$ close to the lattice heat capacity to that of an ideal atomic gas, $3R/2$. Coefficients σ_a and T_a define the characteristic density and temperature of this transition.

The variation of the characteristic temperature defines the vibrational spectrum and reflects the gradual change of the Grüneisen coefficient of the liquid phase from values $\gamma^{(l)} \approx \gamma^{(s)}$, corresponding to condensed states, to the ideal-gas value of $2/3$ in the limit of high temperatures and very low densities. Under these assumptions, the characteristic temperature is given by the approximating formula

$$\theta^{(l)}(V, T) = \sigma^{2/3}T_{sa}\frac{T_{ca}\theta_c^{(l)}(V) + T}{T_{ca} + T}, \tag{20}$$

where the characteristic temperature in the liquid phase is given in a form analogous to Eq. (16)

$$\theta_c^{(l)}(V) = \theta_0^l\exp\left(\frac{(\gamma_{0l} - 2/3)(B_l^2 + D_l^2)}{B_l} \times \arctan\left[\frac{xB_l}{B_l^2 + D_l(x + D_l)}\right]\right). \tag{21}$$

The parameters in Eq. (21), B_l and D_l, are found from shock-wave experiments for solid and porous samples, while the constant θ_0^l is determined by equation $\theta_c^{(l)}(0) = T_{ca}$.

The potential term $F_m(V, T)$ provides for correct values of the entropy changes $\Delta S = \Delta S_{m0}$ and volume changes $\Delta V = \Delta V_{m0}$ on melting at ambient pressure, and disappears in the gas phase. The contribution of F_m should also decrease upon compression due to decreasing differences between

https://doi.org/10.1017/S0263034607000687 Published online by Cambridge University Press

the properties of the solid and liquid phases. These requirements are satisfied by the relation

$$F_m(V, T) = 3R\left(\frac{2\sigma_m^2 T_{m0}}{1+\sigma_m^3}\left[C_m + \frac{3A_m}{5}(\sigma_m^{5/3} - 1)\right] + (B_m - C_m)T\right), \quad (22)$$

where $\sigma_m = \sigma/\sigma_{m0}$ is the relative density of the liquid phase on the melting curve. The constants A_m, B_m, and C_m are uniquely determined by the equilibrium conditions along the melting curve at $T = T_m$.

3.3. Thermal Contribution of Electrons

The electronic thermal contribution has an identical form for the solid and liquid phases. It is given by

$$F_e(V, T) = -c_e(V, T)T \ln\left(1 + \frac{B_e(T)T}{2c_{ei}(V, T)}\sigma^{-\gamma_e(V, T)}\right). \quad (23)$$

It includes the generalized analog of the coefficient of the electronic heat capacity B_e:

$$B_e(T) = \frac{2}{T^2}\int\left(\int_0^T \beta(\tau)d\tau\right)dT, \quad (24)$$

the coefficient of the electronic heat capacity β:

$$\beta(T) = \beta_i + \left(\beta_0 - \beta_i + \beta_m\frac{T}{T_b}\right)\exp(-T/T_b), \quad (25)$$

the heat capacity of the electron gas c_{ei}

$$c_{ei}(V, T) = \frac{3R}{2}\left(Z + \frac{\sigma_z\sigma T_z^2(1-Z)}{(\sigma+\sigma_z)(T^2+T_z^2)}\exp(-\tau_i/T)\right), \quad (26)$$

$$\tau_i = T_i\exp(-\sigma_i/\sigma), \quad (27)$$

and the analog of the electronic Grüneisen coefficient γ_e:

$$\gamma_e(V, T) = \gamma_{ei} + \left(\gamma_{e0} - \gamma_{ei} + \gamma_m\frac{T}{T_g}\right) \times \exp\left(-\frac{T}{Tg} - \frac{(\sigma-\sigma_e)^2}{\sigma\sigma_d}\right). \quad (28)$$

Approximating dependencies are written in this manner to satisfy primarily the asymptotic relations for the electron gas free energy, namely expressions for the degenerate electron gas $F_e(V, T) = -\beta_0 T^2\sigma^{-\gamma_0}/2$ at moderate temperatures ($T \ll T_{Fermi}$) and expressions for an ideal electron gas $F_e(V, T) = 3RZ\ln(\sigma^{2/3}T)/2$ as $T \to \infty$. Here Z is the atomic number and R is the gas constant. The specific forms given for the separate terms of Eq. (23) were chosen to satisfy these requirements.

Eqs. (23)–(28) are written in a form which correctly represents the primary ionization effects in the plasma region and the behavior of the partially ionized metal. Eq. (27) for τ_i describes a decrease of the ionization potential as the plasma density increases, and the constants σ_z and T_z define, respectively, the characteristic density of the "metal-insulator" transition and the temperature dependence of the transition from a singly ionized gas to a plasma with the ion–charge mean value Z.

3.4. EOS Construction Procedure

The set of Eqs. (4)–(28) fully defines the thermodynamic potential for metals over the entire phase diagram for the region of practical interest. Some coefficients in the EOS, included in the analytical expressions, are constants characteristic for each metal (atomic weight and charge, density at normal conditions and other) and are obtained from tabulated data. The rest serve as fitting parameters and their values are found from the optimum description of the available experimental and theoretical data, while providing for correct asymptotes to calculations based on the Debye–Hückel and Thomas–Fermi theories (Kalitkin & Kuzmina, 1975). It should be emphasized that, even though the number of coefficients in Eqs. (4)–(28) is large, most of them are rigidly defined constants whose values are assigned explicitly or implicitly from the fulfillment of various thermodynamic conditions at specific points on the phase diagram. A few coefficients (about 10) serve to characterize the densities and temperatures of transition from one typical phase-plane region to another and are found empirically. The tables in the appendix lists the parameters of the EOS model given by Eqs. (4)–(28) along with the values for aluminum.

The numerous experimental and theoretical data characterizing the thermodynamic properties of metals for a wide range of parameters, was used in determining the numerical values of coefficients in the EOS, This procedure was carried out with the aid of a specially developed computer program using Eqs. (4)–(28) for thermodynamic calculations. At the preliminary stage of calculations, some thermodynamic constants known for each substance (such as normal density, changes in density and entropy at the melting point under normal pressure, cohesion energy, and the like) were used by the program automatically for finding a number of other uniquely defined coefficients (parameters of the cold curve, melting curve, and so on). This further enables one, by way of calculating algebraic or integral relations valid for self-similar hydrodynamic flows, to perform calculations of the kinematic characteristics measured experimentally at high and ultrahigh pressures, namely, the incident and reflected wave velocities and velocities in adiabatic expansion waves (release isentropes), as well as to allow for melting and evaporation effects. The range of action of each fitting parameter that remains free is very localized, as a result of which its value may be selected independently

https://doi.org/10.1017/S0263034607000687 Published online by Cambridge University Press

from a comparison of the calculations with available experimental data.

The EOS was constructed using the following high pressure, high temperature information: measurements of isothermal compressibility in diamond anvil cells, data on sound velocity and density in liquid metals at atmospheric pressure, IEX measurements, data on the shock compressibility of solid and porous samples in incident and reflected shock waves, impedance measurements of shock compressibility using an underground nuclear explosion, data on isentropic expansion of shocked metals, calculations by quantum molecular dynamics (QMD), Debye–Hückel, and Thomas–Fermi models, and evaluations of the critical point.

All of the experimental and theoretical data have a given history of accuracy and reliability. The major problem in EOS construction is to provide for a self-consistent and noncontradictory description of the many kinds of available data.

4. THERMODYNAMIC PROPERTIES OF ALUMINUM

This section presents the calculation results of the thermodynamic properties and the phase diagram of aluminum. This is done with the use of Eqs. (4)–(28). The resulting dependencies are compared with the experimental data and theoretical calculations that are most significant at high pressures and temperatures.

All data are presenting in graphs. Earlier results of Al'tshuler *et al.* (1958*a*, 1958*b*, 1960*a*; McQueen *et al.*, 1970; van Thiel, 1977) have been revised several times. The effects of impactor heating and an attenuation of the shock in the window and specimen have been analyzed (Al'tshuler & Chekin, 1984), and the corrections have been applied based on new precise shock adiabats of reference materials (Marsh, 1980; Zhernokletov *et al.*, 1996; Trunin *et al.*, 2001). The experimental shock wave data in the graphs correspond to the most recent reported values, for which accounting have been made for all of these experimental factors.

The present EOS accounts for the theoretical and experimental data published up to the middle of 2007. The parameters of the liquid state have been changed strongly, in comparison with the predecessor aluminum EOS of Busman *et al.* (1993), to satisfy new high pressure Hugoniot data, isothermal (Akahama *et al.*, 2006) and isentropic compression measurements (Davis, 2006) and the results of quantum molecular dynamic calculations (Desjarlais, personal communication) in the critical point region.

4.1. Crystal

Aluminum has an face-centered cubic (fcc) structure at room pressure and temperature. The structural fcc hexagonal close packed (hcp) phase transition at $T = 0$ K has been predicted by different theories (Voropinov *et al.*, 1970; McMahan & Moriarty, 1983; Lam & Cohen, 1983; Wentzcovich & Law, 1991; Boettger & Trickey, 1996) to occur at pressures of 120–360 GPa. According to (Greene *et al.*, 1994) it remains a simple solid to a pressure of 220 GPa under isothermal compression in a diamond anvil cell, but in analogous experiment (Akahama *et al.*, 2006) at 217 GPa aluminum transforms to *hcp* phase with a volume reduction of 1%. Novel high-pressure data on isentropic compression of aluminum (Davis, 2006), as well as the results of the diamond anvil cell (DAC) experiment of (Greene *et al.*, 1994; Akahama *et al.*, 2006), which are in the solid state region, do not demonstrate dramatic changes in the thermodynamic parameters. So the present EOS provides for a monotonic compression curve.

A comparison of the cold curve, found using Eqs. (5)–(9), with the results of band–structure calculations is shown in Figure 3. It is seen that the elastic curve agrees with different variants of Thomas–Fermi theory (Kalitkin & Kuzmina, 1975; Perrot, 1979), the augmented–plane wave (APW) (McMahan & Ross, 1979), the self–consistent cell model (Liberman, 1979), and the Hartree–Fock–Slater method (Nikiforov *et al.*, 1989), as well in all ranges of densities to 100-fold compression.

The room temperature isotherm to 12 GPa (Syassen & Holzaphel, 1978), 220 GPa (Greene *et al.*, 1994) and 333 GPa (Akahama *et al.*, 2006) is drawn in Figure 4, along with isentropic compression data (Davis, 2006) obtained to 300 GPa. Figure 5 also contains theoretical isotherms calculated with the use of the pseudopotential approach (Nellis *et al.*, 1988) and the full-potential linearized augmented plane wave method (Wang *et al.*, 2000). The compression curve for this EOS, which is an isentrope, is also shown. Note that the difference between the compression isentrope and isotherms, with $T = 0$ and 298 K, in this range of pressures of up to 340 GPa is negligible. The overall agreement between this semi-empirical compression

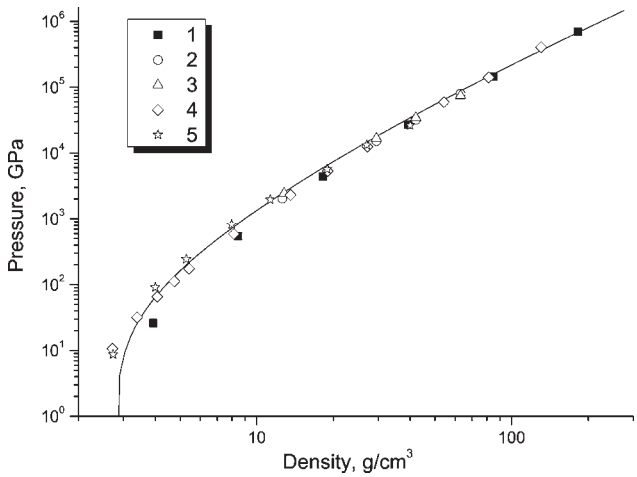

Fig. 3. Pressure in aluminum at $T = 0$ K. Nomenclature: line–EOS; points–theories, 1–Thomas–Fermi model with corrections Kalitkin & Kuzmina (1975), 2–self-consistent cell model Liberman, (1979), 3–APW McMahan & Ross, (1979), 4–Thomas–Fermi model with gradient correction Perrot (1979), 5–modified Hartree–Fock–Slater model Nikiforov *et al.* (1989).

https://doi.org/10.1017/S0263034607000687 Published online by Cambridge University Press

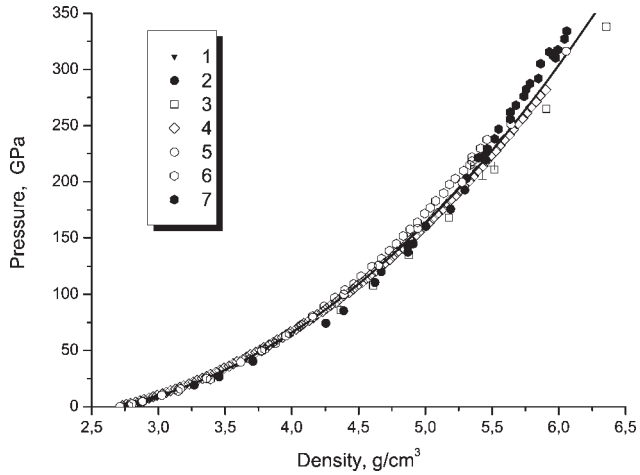

Fig. 4. Pressure in solid aluminum. Nomenclature: line–EOS; points–experiment, 1–DAC Syassen & Holzaphel (1978), 2–DAC Greene *et al.* (1994), 4–isentropic compression Davis (2006), 6,7–DAC *fcc* and *hcp* Akahama *et al.* (2006), and theory, 3–Nellis *et al.* (1988), 5–Wang *et al.* (2000).

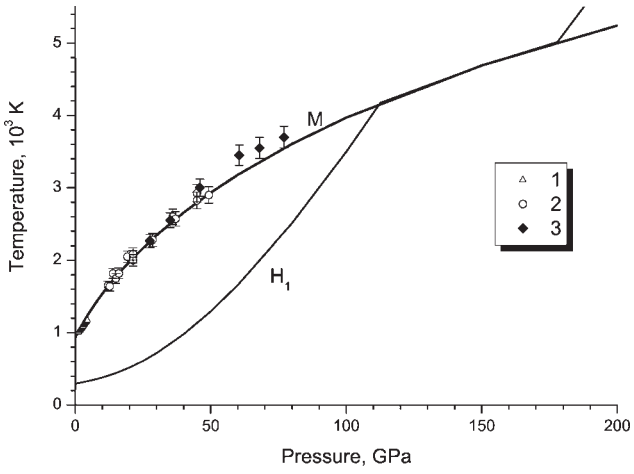

Fig. 6. Aluminum melting at high pressures. Nomenclature: lines–EOS calculations, M–melting, H_1–shock adiabat; points–experiment, 1–Jayaraman *et al.* (1963), 2–Hanstrom & Lazor (2000), 3–Boehler & Ross (1997).

curve and theory and experiment is good and within the error bars of the experimental data.

4.2. Melting

At room pressure, aluminum melts at $T = 933$ K. The experimental data (Hultrgen *et al.*, 1973) at 1 bar are compared with EOS calculations in Figure 5. Less dense liquid states, characterized by higher values of enthalpy, have been measured in an IEX experiment at 0.3 GPa (Gathers, 1983). The calculated $P = 0.3$ GPa isobar is also shown in this figure. Note that these EOS isobars are clearly different, while data at 0.3 GPa (Gathers, 1983) correspond to the linear approximation of 1 bar measurements (Hultrgen *et al.*, 1973). The

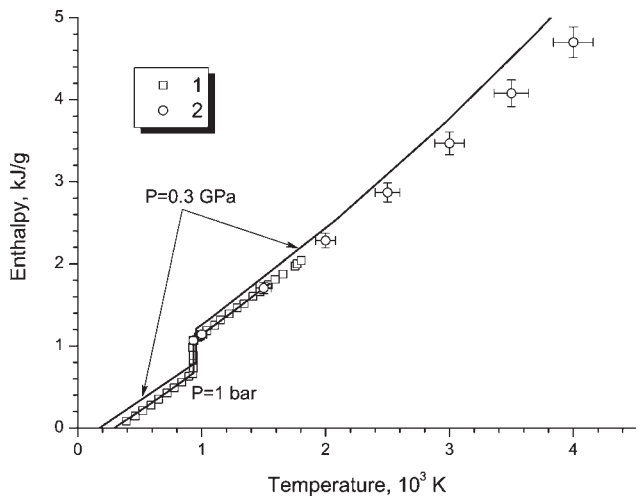

Fig. 5. Aluminum melting at 1 bar and at 0.3 GPa. Nomenclature: line–EOS; points–experiment, 1–at 1 bar Hultrgen *et al.* (1973), 2–at 0.3 GPa Gathers (1983).

analysis of Figure 4 demonstrates the reliability of the developed EOS in this region of the phase diagram.

The high-pressure melting curve is plotted in the pressure-temperature diagram of Figure 6. The extrapolation of static DAC measurements (Boehler & Ross, 1997; Hanstrom & Lazor, 2000) is in good agreement with the results of a dynamic experiment (McQueen *et al.*, 1984), according to which aluminum melts under shock at a pressure of 110 GPa. The calculated melting line and shock adiabat show good agreement with available data.

4.3. Dense Aluminum at High Pressure

In this section, let us discuss the results of shock-wave measurements. Aluminum has been extensively investigated in the past 50 years. Its principal Hugoniot has been measured with the use of traditional high-explosive drivers to pressures of 200 GPa (Al'tshuler *et al.*, 1960*a*; McQueen *et al.*, 1970; Al'tshuler *et al.*, 1981; Marsh, 1980). Light-gas guns allowed one to obtain precise data to pressures of 210 GPa (Isbell *et al.*, 1968; Mitchell & Nellis, 1981). Much higher pressures of 400 GPa were accessed with the use multi-layer cumulative explosive systems (Glushak *et al.*, 1989) and pressures of 990 GPa with the use of powerful hemi-spherical cumulative drivers (Skidmore & Morris, 1962; Kormer *et al*, 1962; Al'tshuler & Chekin, 1984; Trunin, 1986; Trunin *et al.,* 1995*a*, 1995*b*). High-precision data up to 480 GPa were measured in Z–pinch experiments (Knudson *et al.*, 2003), in which aluminum flyer plates were magnetically accelerated to high velocities.

Extreme pressures in aluminum were generated with the use of underground nuclear explosions. Maximum pressures of 400 TPa were realized (Vladimirov *et al.*, 1984), along with the shock limit of compression ratio. One should specially note that at higher pressures, the contribution of

https://doi.org/10.1017/S0263034607000687 Published online by Cambridge University Press

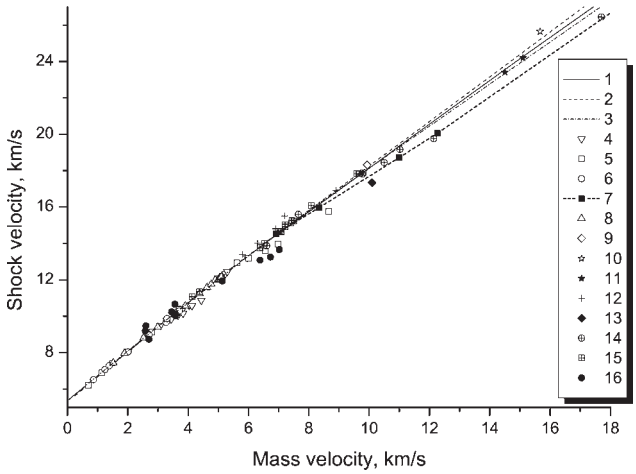

Fig. 7. Aluminum shock adiabat. Nomenclature: lines–EOS calculations, 1–this work, 2–EOS Kerley (1987), 3–QMD Desjarlais, (2006); points–experiment, 4–Isbell *et al.* (1968), 5–Al'tshuler *et al.* (1960*a*); Al'tshuler & Chekin (1984), 6–Al'tshuler *et al.* (1981), 7–Al'tshuler *et al.* (1977), 8–Mitchell & Nellis (1981), 9–Kormer *et al.* (1962), 10–Volkov *et al.* (1981), 11–Simonenko *et al.* (1985), 12–Glushak *et al.* (1989), 13–Trunin (1986), 14–revision Trunin *et al.* (2001) of data Avrorin *et al.* (1987), 15–Knudson *et al.* (2003), 16–Skidmore & Morris (1962).

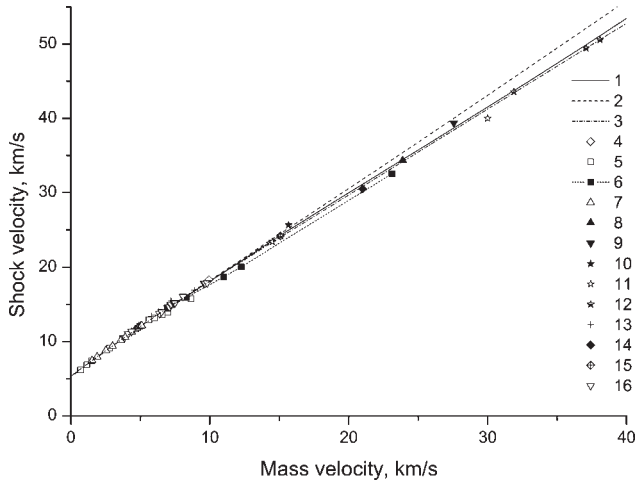

Fig. 8. Aluminum shock adiabat at extreme pressures. Nomenclature: lines–EOS calculations, 1–this work, 2–EOS Kerley (1987), 3–QMD Desjarlais (2006); points–experiment, 4–Kormer *et al.* (1962), 5–Al'tshuler *et al.* (1960*a*); Al'tshuler & Chekin (1984), 6–Al'tshuler *et al.* (1977), 7–Mitchell & Nellis (1981), 8–Ragan (1982), 9–Ragan (1984), 10–Volkov *et al.* (1981), 11–Simonenko *et al.* (1985), 12–Avrorin *et al.* (1986), 13–Glushak *et al.* (1989), 14–Podurets *et al.* (1994), 15–Trunin *et al.* (1995*a*), 16–Knudson *et al.* (2003).

radiation to the pressure and energy will be more significant than the thermal contributions. So we may conclude that the EOS limit for the aluminum shock adiabat has been achieved. Absolute measurements of aluminum shock compressibility were done at 0.9–3.2 TPa (Simonenko *et al.*, 1985). All other measurements are referred to as nuclear impedance measurements (NIM), which are limited in the accuracy with which a reference material is known. In these works, aluminum's compressibility was studied with respect to different standard materials: quartz to pressures of 0.27–2 TPa (Al'tshuler *et al.*, 1977), molybdenum at 2.2–2.9 TPa (Ragan, 1982, 1984), and iron at 4.3–28.9 TPa (Avrorin *et al.*, 1986), 1.7 TPa (Podurets *et al.*, 1994), and 0.25–1.27 TPa (revision Trunin *et al.*, 2001) of data in Avrorin *et al.*, 1987).

Because the structural *fcc–hcp* phase transition seemed to have confirmed in shock wave experiments (Al'tshuler & Bakanova, 1968; see data points Al'tshuler *et al.*, 1960*a*; Al'tshuler & Checkin, 1984; Skidmore & Morris, 1962; Isbell *et al.*, 1968; Trunin, 1986; Fig. 7), for some times, investigators used the "soft" shock adiabat at pressures greater than 200 GPa, taking into account this transition effect (see absolute point Trunin (1986) and NIM data Al'tshuler *et al.* (1977); Trunin *et al.* (1995*b*)). More recent high-pressure experiments (Glushak *et al.*, 1989), the revision Trunin *et al.* (2001) of data in Avrorin *et al.* (1987), and, especially, precise measurements (Knudson *et al.*, 2003) and QMD calculations (Desjarlais, personal communication), demonstrate a "stiffer" behavior of the aluminum principal Hugoniot. The present EOS describes reliable shock wave data. At high pressure it has an intermediate position between the semi-empirical EOS of Kerley (1987) and novel QMD results (Desjarlais, personal communication). The calculated shock adiabat is also compared against experimental data and theoretical Hugoniots at extreme pressures in Figure 8. This region corresponds to NIM measurements obtained with a highly reliable iron standard to pressures of 10 TPa. These data served to fit the thermal contribution of electrons to the EOS.[1]

Figure 9 illustrates the phase diagram of aluminum in a pressure–density. States of lower density in comparison with the principal Hugoniot have been investigated by shock compression of porous aluminum samples in the megabar range of pressures (Kormer *et al.*, 1962; Bakanova *et al.*, 1974; van Thiel, 1977; Trunin *et al.*, 2001). The presence of these data allows an accurate fit of the thermal contribution of atoms to the EOS. The analysis of Figure 9 demonstrates the reliability of the present EOS in regions of the phase diagram which are far from the principal Hugoniot. Note that the sound speed in shocked metal is also described with high accuracy, see Figure 9a. Analogous agreement has also been obtained after comparison with megabar–pressure data on double and triple compression of aluminum in reflected shock waves (Al'tshuler & Petrunin, 1961; Neal, 1976; Nellis *et al.*, 1988, 2003).

4.4. Aluminum at Lower Densities

The value of shock pressure or, more strictly, of entropy in shocked materials, influences how far a material expands with passage of a release wave. EOS calculations show that

[1] Numerous data from the compendium (March, 1980) (ca. 250 points) are not shown in Figures. 7 and 8, because in this region to 120 GPa the shock adiabat is well determined.

https://doi.org/10.1017/S0263034607000687 Published online by Cambridge University Press

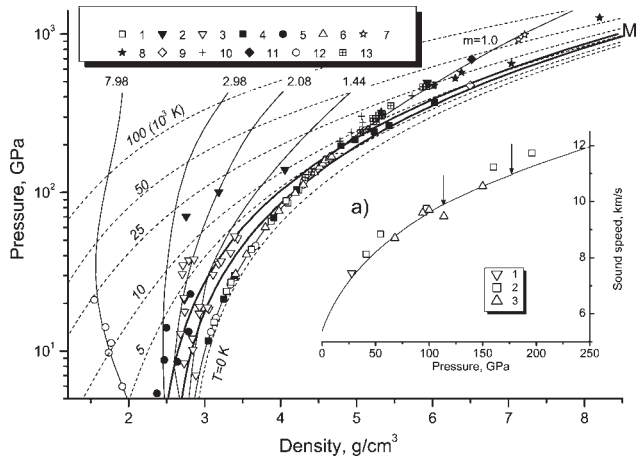

Fig. 9. Phase diagram of aluminum at high pressures. Nomenclature: lines–EOS calculations, T–isotherms, M–melting region, m–shock adiabats of porous samples ($m = \rho_0/\rho_{00}$–porosity); points–experimental data, 1–Al'tshuler *et al.* (1981), 2–Kormer *et al.* (1962), 3–van Thiel (1977); 4–Al'tshuler *et al.* (1960*a*); Al'tshuler & Chekin (1984), 5–Bakanova *et al.* (1974), 6–Mitchell & Nellis (1981), 7–Simonenko *et al.* (1985), 8–revision Trunin *et al.* (2001) of original data Avrorin *et al.* (1987), 9–Trunin (1986), 10–Glushak *et al.* (1989), 11–Trunin *et al.* (1995*a*), 12–Trunin *et al.* (2001), 13–Knudson *et al.* (2003). a) Sound speed in shocked aluminum. Line–EOS, points-experiment, 1–Neal (1975), 2–Al'tshuler *et al.* (1960*b*), 3–McQueen *et al.* (1984), arrows indicate the melting region.

nothing special happens with aluminum in adiabatic–expansion experiments done in the range of shock pressures from 8–200 GPa (Bakonova *et al.*, 1983; Zhernokletov *et al.*, 1995). These data are shown in Figure 10. Here initial Hugoniot states correspond to solid or melted aluminum. Final states of the release isentropes have been measured under the condition of expansion into air.

Figure 11 illustrates the expansion process in which, according to the present EOS, shocked aluminum is liquid. Again,

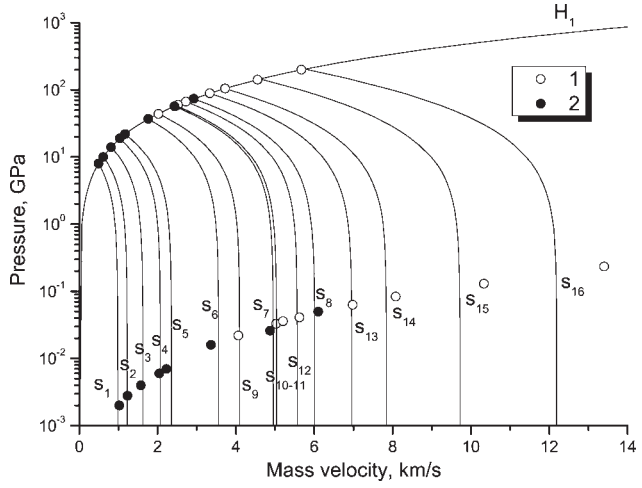

Fig. 10. Release isentropes of solid and melted aluminum. Nomenclature: lines–EOS calculations, H_1–principal Hugoniot, s_i–release isentropes; points–experiment, 1–Bakanova *et al.* (1983), 2–Zhernokletov *et al.* (1995).

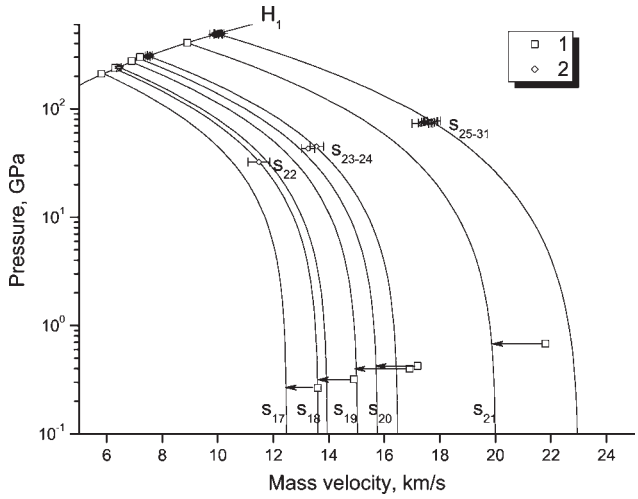

Fig. 11. Release isentropes of liquid aluminum. Nomenclature: lines–EOS calculations, H_1–principal Hugoniot, s_i–release isentropes; points–experiment, 1–expansion into air Glushak *et al.* (1989), 2–expansion into aerogel Kundson *et al.* (2005).

EOS calculations are compared against experimental isentropes (Glushak *et al.*, 1989; Knudson *et al.*, 2005). At higher pressure one can see from Figures 10 and 11 that the calculated isentropes s_{15}–s_{21} deviate from the experimental data for expansion into air (Bakanova *et al.*, 1983; Glushak *et al.*, 1989) in a non–systematic way. In contrast, the agreement with isentropes s_{22}–s_{31} expanded into aerogel (Knudson *et al.*, 2005) is very good, see Figure 11. Like isentropes s_1–s_{16} from Figure 10, all the isentropes s_{17}–s_{31} show a monotonic dependence at all investigated pressures.

All the release isentropes for aluminum s_1–s_{31} from experiments (Bakanova *et al.*, 1983; Zhernokletov *et al.*, 1995; Glushak *et al.*, 1989; Knudson *et al.*, 2005) are

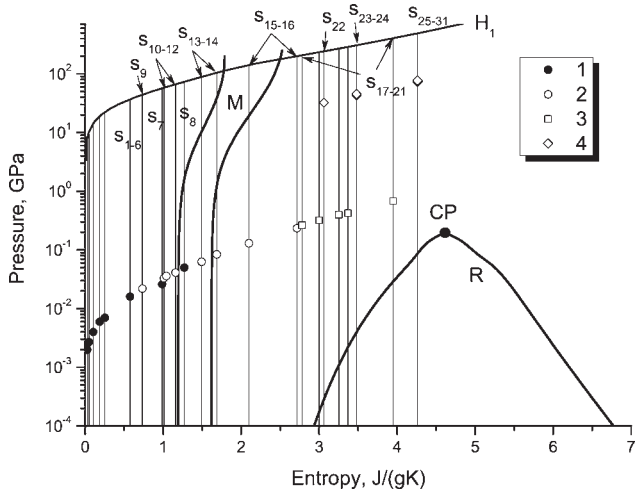

Fig. 12. Pressure–entropy diagram for aluminum. Nomenclature: lines–EOS calculations, H_1–principal Hugoniot, M–melting region, R–liquid–gas region with the critical point CP, s_i–release isentropes (see Figs. 10, 11); points–experiment, 1–Zhernokletov *et al.* (1995), 2–Bakanova *et al.* (1983), 3–Glushak *et al.* (1989), 4–Knudson *et al.* (2005).

https://doi.org/10.1017/S0263034607000687 Published online by Cambridge University Press

presented in Figure 12. It is interesting to note, the positions of these release isentropes in the phase space. In the experiments of Bakonova *et al.* (1983) and Zhernokletov *et al.* (1995), isentropes s_1-s_7 and $s_{10}-s_{12}$ are in the solid state, isentropes s_8 and s_{13} originate in the solid state and end in the melting region, while the isentrope s_{14} starts in the solid and ends in the liquid. Isentropes $s_{15}-s_{16}$ are mainly in the liquid state. Higher shock pressures, and consequently higher entropies, achieved in the experiments of Glushak *et al.* (1989) and Knudson *et al.* (2005) result in all isentropes $s_{17}-s_{31}$ occupying a region of the liquid state. The analysis of the position of the two-phase liquid-gas region with respect to the shock adiabat of air, see line *R* and points in Figure 12, shows that aluminum does not and will not evaporate upon adiabatic expansion from shocked states into air.

Density measurements at $P = 1$ bar are available for solid (Toloukian *et al.*, 1975) and liquid (Lang, 1995) aluminum at lower densities. Thermophysical properties of the liquid aluminum have been studied at $P = 0.3$ GPa in an isobaric expansion experiment (Gathers, 1983). EOS calculations are compared against these data and different evaluations of the critical point in Figure 13. This figure demonstrates that the present EOS describes the experimental points with outstanding accuracy. The EOS parameters of the critical point, $P_c = 0.197$ GPa, $T_c = 6250$ K, and $V_c = 1.423$ cm^3/g, agree with QEOS parameters $P_c = 0.168$ GPa, $T_c = 5520$ K (Young & Corey, 1995) and are also very closely in density with the other evaluations. This position of the critical point in the present EOS provides for an accurate description of IEX data (Gathers, 1983), see the 0.3 GPa isobar in Figure 13. The calculated evaporation temperature at room pressure, $T_V = 2770$ K, coincides with the tabulated value (Hultrgen *et al.*, 1973).

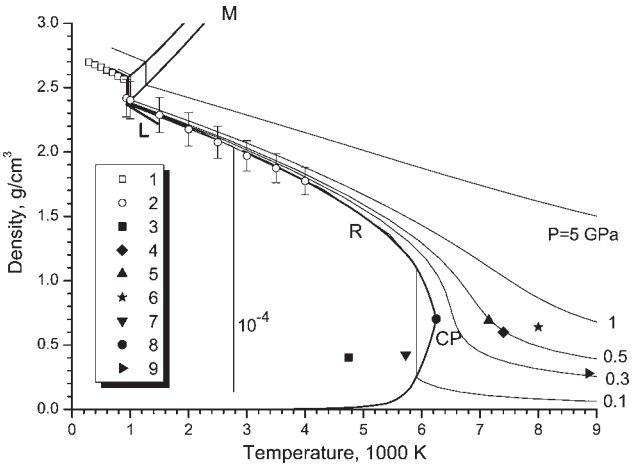

Fig. 13. Phase diagram of aluminum at lower densities. Nomenclature: lines–EOS calculations, M–melting region, R–liquid-gas region with the critical point CP, P–isobars, and L–density of liquid metal at 1 bar Lang (1994–1995); points–experiment, 1–Toloukian *et al.* (1975), 2–Gathers (1983), and evaluations of the critical points, 3–Gates & Thodos (1960), 4–Morris (1964), 5–Young & Alder (1971), 6–Fortov & Yakubov (1999), 7–Gathers (1986), 8–this work, 9–Likalter (2002).

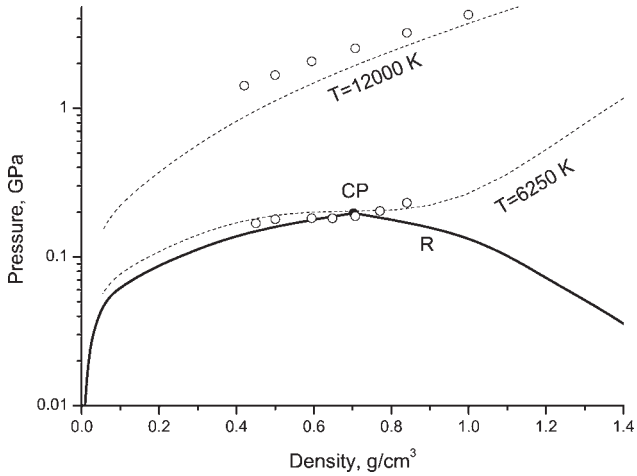

Fig. 14. Pressure–density diagram of aluminum's critical region. Nomenclature: lines–EOS calculations, R–liquid–gas region with the critical point CP, T–isotherms; open circles–QMD calculations Desjarlais (2006).

EOS isotherms are compared with QMD calculations (Desjarlais, personal communication) in Figure 14. The EOS critical isotherm at $T = 6250$ K describes the QMD results very well; the density of the critical point is also very close to the QMD result. The isotherm at $T = 12000$ K also shows good agreement with the QMD calculations.

Experimental isochors of heated aluminum (Renaudin *et al.*, 2003) occupy the super critical domain on the phase diagram. EOS isochors and the isochore 0.1 g/cm^3 from Saha plasma model (Gryaznov *et al.*, 1998) are drawn in Figure 15, together with experimental points. The comparison with other advanced theoretical models is also available in the original work (Renaudin *et al.*, 2003).

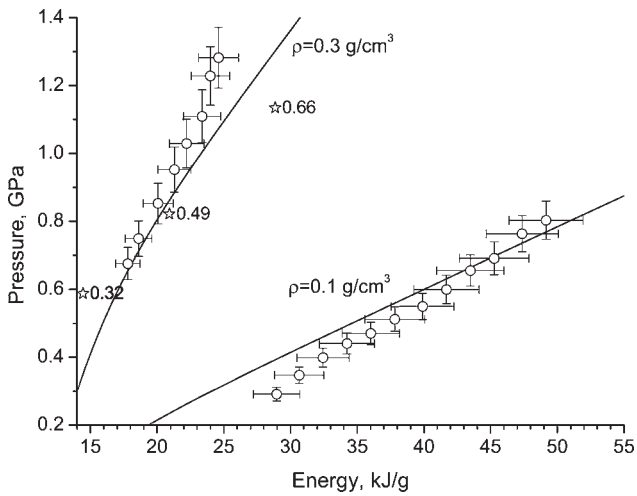

Fig. 15. Pressure–energy diagram of isochorically heated aluminum. Nomenclature: lines–EOS calculations, points with bars–EPI experiment Renaudin *et al.* (2003), open stars–Saha model Gryaznov *et al.* (1998) (numbers near stars indicate ionization ratio).

https://doi.org/10.1017/S0263034607000687 Published online by Cambridge University Press

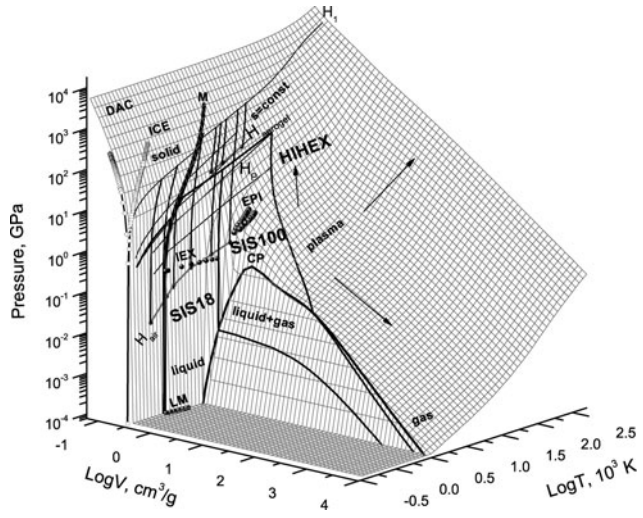

Fig. 16. Generalized 3D volume-temperature-pressure surface for aluminum. M–melting region; R–boundary of two-phase liquid-gas region with the critical point CP; H_1 and H_p–principal and porous Hugoniots; H_{air} and $H_{aerogel}$ – shock adiabats of air and aerogel; DAC–diamond-anvil-cells data; ICE–isentropic compression experiment; IEX–isobaric expansion data; S–release isentropes; HIHEX–region accessible with use of intense heavy ion beams SIS18 and SIS100 (see for details Hoffman *et al.* (2002); Tahir *et al.* (2005*a*)). Phase states of the metal are also shown.

Finally, the summary of all mentioned above experimental data is given in 3D pressure–volume–temperature surface in Figure 16. It is worth to underline good potential capabilities of intense heavy ion beams for inducing high-energy-density states in expanded aluminum. In this region of practical interest and importance, we have today limited amount of a data for testing and calibrating modern theoretical models.

5. CONCLUSION

New advanced studies of aluminum properties at extreme conditions include experiments and theoretical calculations. Experimental investigations of isothermal, shock and isentropic compression of aluminum at high pressures up to 500 GPa have demonstrated behavior that results in a more "stiff" compression curve and shock adiabat for aluminum than was previously figured. Adiabatic-expansion measurements of shocked aluminum have brought new accurate data for the hot expanded liquid. Theoretical "ab initio" QMD calculations in the vicinity of the critical point have established the reference domain of thermodynamic data.

These data serve as a fundamental basis for the new multiphase EOS for aluminum presented in this paper. It accounts for the high pressure, high temperature experimental, and theoretical data that was available up to the middle of 2007. The compression curve and the principal Hugoniot in the resulting EOS are fit to new data, as well as the critical point. According to the EOS model, shocked aluminum melts at 113 GPa and the parameters of the critical point are: $P_c = 0.197$ GPa, $T_c = 6250$ K, and $V_c = 1.423$ cm^3/g.

The developed EOS describes with high accuracy and reliability a broad range of the phase diagram, from the high-pressure shocked metal to more dense states in reflected shock waves and to regions of the phase diagram with much lower densities accessed in the process of the adiabatic expansion of shocked metal. The high accuracy suits this EOS to be applied in advanced numerical modeling for solving numerous problems in the physics of high energy densities. The developed EOS together with QMD data provides for self-consisted description of both thermodynamic and transport properties of aluminum.

ACKNOWLEDGMENTS

We acknowledge Dr. M. P. Desjarlais for discussions and presented QMD-data and Dr. V. K. Gryaznov for results of Saha EOS calculations. The work was performed by support from Visiting Research Scholars Program at Sandia National Laboratories. Sandia is a multiprogram laboratory operated by Sandia Corporation, a Lockheed Martin Company, for the United States Department of Energy's National Nuclear Security Administration under contract DE-AC04-94AL85000.

REFERENCES

Akahama, Y., Nishimura, M., Kinoshita, K. & Kawamura, H. (2006). Evidence of a fcc-hcp transition in aluminum at multimegabar pressure. *Phys. Rev. Lett.* **96**, 045505–1–045505–4.

Al'tshuler, L.V. (1965). Use of shock waves in physics of high pressure. *Sov. Phys. Usp.* **8**, 52–91.

Al'tshuler, L.V. & Bakanova, A.A. (1968). Electronic structure and compressibility of metals at high pressures [in russian]. *Usp. Fiz. Nauk.* **95**, 193–215.

Al'tshuler, L.V., Bakanova, A.A., Dudoladov, I.P., Dynin, E.A., Trunin, R.F. & Chekin, B.S. (1981). Shock adiabatic curves for metals. new data, statistical analysis and general laws. *J. Appl. Mech. Techn. Phys.* **22**, 145–169.

Al'tshuler, L.V. & Chekin, B.S. (1984). Metrology of high pulsed pressures [in russian]. In *Proceed.-s 1 Soviet Union Symposium on High Pressures*, pp. 5–22. Moskva: VNIIFTRI.

Al'tshuler, L.V., Kalitkin, N.N., Kuz'mina, L.V. & Chekin, B.S. (1977). Shock adiabats for ultrahigh pressures. *Sov. Phys. JETP* **45**, 167–171.

Al'tshuler, L.V., Kormer, S.B., Bakanova, A.A. & Trunin, R.F. (1960*a*). Equations of state for aluminum, copper and lead in the high pressure region. *Sov. Phys. JETP* **11**, 573–579.

Al'tshuler, L.V., Kormer, S.B., Brazhnik, M.I., Vladimirov, L.A., Speranskaya, M.P. & Funtikov, A.I. (1960*b*). The isentropic compressibility of aluminum, copper, lead at high pressures. *Sov. Phys. JETP* **11**, 766–775.

Al'tshuler, L.V., Krupnikov, K.K. & Brazhnik, M.I. (1958*a*). Dynamical compressibility of metals under pressure from 400000 to 4 million atmospheres. *Sov. Phys. JETP* **34**, 614–618.

Al'tshuler, L.V., Krupnikov, K.K., Ledenev, B.N., Zhuchikhin, V.I. & Brazhnik, M.I. (1958*b*). Dynamical compressibility and equation of state for iron under high pressure. *Sov. Phys. JETP* **7**, 606–613.

https://doi.org/10.1017/S0263034607000687 Published online by Cambridge University Press

Al'tshuler, L.V., Moiseev, B.N., Popov, L.V., Simakov, G.V. & Trunin, R.F. (1968). Relative compressibility of iron and lead at pressures of 31 to 34 Mbar. *Sov. Phys. JETP* **27**, 420–422.

Al'tshuler, L.V. & Petrunin, A.P. (1961). Rentgenographic investigation of compressibility of light substances under obstacle impact of shock waves [in russian]. *Zhurn. Tekhn. Fiz.* **31**, 717–725.

Avrorin, E.N., Vodolaga, B.K., Simonenko, V.A. & Fortov, V.E. (1990). *Powerful Shock Waves and Extreme States of Matter* [in Russian]. Moskva: IVTAN.

Avrorin, E.N., Vodolaga, B.K., Voloshin, N.P., Kovalenko, G.V., Kuropatenko, V.F., Simonenko, V.A. & Chernodolyuk, B.T. (1987). Experimental study of the influence of electron shel structure on shock adiabats of condensed metals. *Sov. Phys. JETP Lett.* **66**, 347–354.

Avrorin, E.N., Vodolaga, B.K., Voloshin, N.P., Kuropatenko, V.F., Kovalenko, G.V., Simonenko, V.A. & Chernodolyuk, B.T. (1986). Experimental investigation of shell effects on the shock adiabats of aluminum and lead. *Sov. Phys. JETP Lett.* **43**, 93–96.

Bakanova, A.A., Dudoladov, I.P. & Sutulov, Yu.N. (1974). Shock compressibility of porous tungsten, molybdenum, copper, and and aluminum in low pressure range. *J. Appl. Mech. Techn. Phys.* **15**, 241.

Bakanova, A.A., Dudoladov, I.P., Zhernokletov, M.V., Zubarev, V.N. & Simakov, G.V. (1983). On evaporation of shock–compressed metals under expansion. *J. Appl. Mech. Techn. Phys.* **24**, 204.

Birch, F. (1968). On the possibility of large changes in the earth's volume. *Phys. Earth Planet Interiors* **1**, 141–147.

Boehler, R. & Ross, M. (1997). Melting curve of aluminum in diamond cell to 0.8 Mbar: implications for iron. *Earth Planet. Sci. Lett.* **153**, 223–227.

Boettger, J.C. & Trickey, S.B. (1996). High-precision calculation of the equation of state and crystallographic phase stability for aluminum. *Phys. Rev. B* **53**, 3007–3012.

Bushman, A.V. & Fortov, V.E. (1983). Model equations of state. *Sov. Phys. Usp.* **26**, 465–496.

Bushman, A.V., Kanel, G.I., Ni, A.L. & Fortov, V.E. (1993). *Thermophysics and Dynamics of Intense Pulse Loadings*. London: Taylor & Fransis.

Bushman, A.V., Lomonosov, I.V. & Fortov, V.E. (1992). *Equations of State for Metals at High Energy Density [in Russian]. Chernogolovka*: Moscow: Institute of Problems of Chemical Physics.

Carnahan, N.F. & Starling, K.E. (1969). Equation of state for non-attracting rigid spheres. *J. Chem. Phys.* **51**, 635–636.

Chisolm, E.D., Crockett, S.D. & Wallace, D.C. (2003). Test of a theoretical equation of state for elemental solids and liquids. *Phys. Rev. B* **68**, 04103-1-104103-12.

Danson, C.N., Brummitt, P.A., Clarke, R.J., Collier, I., Fell, B., Frackiewicz, A.J., Hawkes, S., Hernandez-Gomez, C., Holligan, P., Hutchinson, M. H.R., Kidd, A., Lester, W.J., Musgrave, I.O., Neville, D. Neely, D.R., Norreys, P.A., Pepler, D.A., Reason, C., Shaikh, W., Winstone, T.B., Wyatt, R. W.W. & Wyborn, B.E. (2005). Vulcan petawatt: Design, operation and interactions at 5×10^{20} wcm-2. *Laser Part. Beams* **23**, 23–30.

Davis, J.-P. (2006). Experimental measurement of the principal isentrope for aluminum 6061-T6 to 240 GPa. *J. Appl. Phys.* **99**, 103512–1–103512–6.

Desai, T., Dezulian, R. & Batani, D. (2007). Radiation effects on shock propagation in Al target relevant to equation of state measurements. *Laser Part. Beams* **25**, 23–30.

Duvall, G.E. & Graham, R.A. (1977). Phase transitions under shock-wave loading. *Rev. Mod. Phys.* **49**, 523–579.

Eliezer, S., Ghatak, A.K. & Hora, H. (1986). *An Introduction to Equations of State: Theory and Applications*. Cambridge: Cambridge Univ. Press.

Eliezer, S., Murakami, M. & Val, J.M. Martinez. (2007). Equation of state and optimum compression in inertial fusion energy. *Laser Part. Beams* **25**, this issue.

Fortov, V.E. & Yakubov, I.T. (1999). *Physics of Nonideal Plasmas*. London: World. Science Publishing Co.

Gates, D.S. & Thodos, D. (1960). The critical constants of the elements. *Am. Inst. Chem. Eng. J.* **6**, 50.

Gathers, G.R. (1983). Thermophysical properties of liquid copper and aluminum. *Int. J. Thermophys.* **4**, 209–226.

Gathers, G.R. (1986). Dynamic methods for investigating thermophysical properties of matter at very high temperatures and pressures. *Rep. Progr. Phys.* **49**, 341–396.

Glushak, B.L., Zharkov, A.P., Zhernokletov, M.V., Ternovoi, V.Ya., Filimonov, A.S. & Fortov, V.E. (1989). Experimental investigation of the thermodynamics of dense plasmas formed from metals at high energy concentrations. *Sov. Phys. JETP* **69**, 739–749.

Greene, R.G., Luo, H. & Ruoff, A.L. (1994). Al as simple solid: high pressure study to 220 GPa (2.2 Mbar). *Phys. Rev. Lett.* **73**, 2075–2078.

Grüneisen, E. (1912). Theorie des festen zustandes einatomiger elemente. *Ann. d. Physik* **39**, 257–306.

Gryaznov, V.K., Fortov, V.E., Zhernokletov, M.V., Simakov, G.V., Trunin, R.F., Trusov, L.I. & Iosilevski, I.L. (1998). Shock compression and thermodynamics of highly nonideal metallic plasma. *JETP* **87**, 678–690.

Hanstrom, A. & Lazor, P. (2000). High pressure melting and equation of state of aluminum. *Earth Planet. Sci. Lett.* **305**, 209–215.

Hoffmann, D. H.H., Blazevic, A., Ni, P., Rosmej, O., Roth, M., Tahir, N.A., Tauschwitz, A., Udrea, S., Varentsov, D., Weyrich, K. & Maronn, Y. (2005). Present and future prospectives for high energy density physics with intense heavy ion and laser beams. *Laser Part. Beams* **23**, 47–33.

Hoffmann, D. H.H., Fortov, V.E., Lomonosov, I.V., Mintsev, V., Tahir, N.A., Varentsov, D. & Wieser, J. (2002). Unique capabilities of an intense heavy ion beam as a tool for equation-of-state studies. *Phys. Plasmas* **9**, 3651–3655.

Holian, K.S. (1986). A new equation of state for aluminum. *J. Appl. Phys.* **59**, 149–157.

Hultrgen, R., Desai, P.D., Hawkins, D.T., Gleiser, M., Kelley, K.K. & Wagman, D.D. (1973). *Selected Values of the Thermodynamic Properties of the Elements*. Metals Park, Ohio: American Society for Metals.

Isbell, W.H., Shipman, F.H. & Jones, A.H. (1968). Hugoniot equation of state measurements for eleven materials to five megabars. Report MSL-68-13. General Motors Corp., Mat. Sci. Lab.

Jayaraman, A., Klement, W. & Kennedy, J.C. (1963). Melting and polymorphic transitions for some Group II–VI compaunds at high pressures. *Phys. Rev.* **130**, 2277–2283.

Jungwirth, K. (2005). Recent highlights of the PALS research program. *Laser Part. Beams* **23**, 177–182.

Kalitkin, N.N. & Kuzmina, L.V. (1975). Tables of thermodynamic properties of matter at high energy densities. Reprint [in Russian] N35. Inst. Prikl. Matem. Akad. Nauk SSSR, Moskva.

Kerley, G.I. (1987). Theoretical equation of state for aluminum. *Intern. J. Impact Eng.* **5**, 441–449.

Knudson, M.D., Asay, J.R. & Deeney, C. (2005). Adiabatic release measurements in aluminum from 240- to 500-GPa states on the principal Hugoniot. *J. Appl. Phys.* **97**, 073514-1-073514-14.

Knudson, M.D., Lemke, R.W., Hayes, D.B., Hall, C.A., Deeney, C. & Asay, J.R. (2003). Near-absolute Hugoniot measurements in aluminum to 500 GPa using a magnetically accelerated flyer plate technique. *J. Appl. Phys.* **94**, 4420–4431.

Kormer, S.B., Funtikov, A.I., Urlin, V.D. & Kolesnikova, A.N. (1962). Dynamical compression of porous metals and the equation of state with variable specific heat at high temperatures. *Sov. Phys. JETP* **15**, 477–488.

Lam, P.K. & Cohen, M.L. (1983). Calculation of high pressure phases of Al. *Phys. Rev. B* **27**, 5986–5991.

Lang, G. (1995). Density of liquid elements. In *CRC Handbook of Chemistry and Physics* (Lide, D.R. Ed.) pp. 4–134. London: CRC Press.

Liberman, D. (1979). Report LA-UR-77-15950. Los Alamos National Laboratory.

Likalter, A.A. (2002). Critical points of metals of three main groups and selected transition metals. *Physica A* **311**, 137–149.

Marsh, S.P., ed. (1980). *LASL Shock Hugoniot Data*. Berkeley: Universiy of California Press.

McMahan, A. & Ross, M. (1979). Report UCRL-79015. Livermore: Lawrence Livermore Lab.

McMahan, A.K. & Moriarty, J.A. (1983). Structural phase stability in in third-period simple metals. *Phys. Rev. B* **27**, 3235–3251.

McQueen, R.G., Fritz, J.N.Morris, C.E. (1984). The velocity of sound behind strong shock waves in 2024 Al. In *Shock Waves in Condensed Matter - 83* (ed. J.R. Asay, R.A. Graham & G.K. Straub), pp. 95–98. Amerstdam: North Holland.

McQueen, R.G., Marsh, S.P., Taylor, J.W., Fritz, J.N. & Carter, W.J. (1970). The equation of state of solids from shock wave studies. In *High Velocity Impact Phenomena* (ed. R. Kinslow), pp. 293–417. New York: Academic Press.

Mitchell, A.C. & Nellis, W.J. (1981). Shock compression of aluminum, copper and tantalum. *J. Appl. Phys.* **52**, 3363–3374.

Morris, E. (1964). An application of the theory of corresponding states to the prediction of the critical constants of metals. Report 0-67/64. London: AWRE.

Neal, T. (1975). Mach waves and reflected rarefactions in aluminum. *J. Appl. Phys.* **46**, 2521–2527.

Neal, T. (1976). Dynamic determination of the Grüneisen coefficient in aluminum and aluminum alloys for densities up to 6 Mg/m^3. *Phys. Rev. B* **14**, 5172–5181.

Nellis, W.J., Mitchell, A.C. & Young, D.A. (2003). Equation-of-state measurements for aluminum, copper, and tantalum in the pressure range 80–440 GPa (0.8–4.4 Mbar). *J. Appl. Phys.* **93**, 304–310.

Nellis, W.J., Moriarty, J.A., Mitchell, A.C., Ross, M., Dandrea, R.G., Ashcroft, N.W., Holmes, N.C. & Gathers, R.G. (1988). Metals physics at ultrahigh pressure: Aluminum, copper and lead as prototypes. *Phys. Rev. Lett.* **60**, 1414–1447.

Nikiforov, A.F., Novikov, V.G. & Uvarov, V.B. (1989). Modified Hartree–Fok–Slater model and its application for obtaining equation of state of matter at high temperatures [in russian]. In *Mathematical Modeling. Physical-Chemical Properties of Matter*. Moskva: Nauka.

Pant, H.C., Shukl, M., Pandey, H.D., Kashyap, Y., Sarkar, P.S., Sinha, A., Senecham, V.K. & Godwal, B.K. (2006). Enhancement of laser induced shock pressure in multilayer solid targets. *Laser Part. Beams* **24**, 169–174.

Peng, H.S., Zhang, W.Y., Zhang, X.M., Tang, Y.J., Zheng, W.G., Zheng, Z.J., Wei, X.F., Ding, Y.K., Gou, Y., Zhou, S.P. & Pei, W.B. (2005). Progress in ICF programs at CAEP. *Laser Part. Beams* **23**, 205–209.

Perrot, F. (1979). Zero-temperature equation of state for metals in the statistical model with density gradient correction. *Physica A* **98**, 555–565.

Podurets, M.A., Ktitorov, V.M., Trunin, R.F., Popov, L.V., Matveev, A.Ya., Pechenkin, B.V. & Sevast'yanov, A.G. (1994). Shock wave compression of aluninum at pressures of 1.7 TPa [in russian]. *Teplofiz. Vys. Temp.* **32**, 952–955.

Ragan, C.E. (1982). Shock compression measurements at 1 to 7 TPa. *Phys. Rev. Ser. A* **25**, 3360–3375.

Ragan, C.E. (1984). Shock-wave experiment at threefold compression. *Phys. Rev. Ser. A* **29**, 1391–1402.

Ray, A., Srivastava, M.K., Kondayya, G. & Menon, S. V.G. (2006). Improved equation of state of metals in the liquid-vapor region. *Laser Part. Beams* **24**, 437–445.

Renaudin, P., Blancard, C., Clerouin, J., Faussurier, G., Noiret, P. & Recoules, V. (2003). Aluminum equation-of-state data in the warm dense matter regime. *Phys. Rev. Lett.* **91**, 075002-1-075002-4.

Ross, M. (1985). Matter under extreme conditions of temperature and pressure. *Rep. Progr. Phys.* **48**, 1–52.

Sasaki, T., Yano, Y., Nakajima, M., Kawamura, T. & Horioka, K. (2006). Warm-dense-matter studies using pulse-powered wire discharges in water. *Laser Part. Beams* **24**, 371–380.

Simonenko, V.A., Voloshin, N.P., Vladimirov, A.S., Nagibin, A.P., Nogin, V.P., Popov, V.A., Sal'nikov, V.A. & Shoidin, Yu.A. (1985). Absolute measurements of shock compressibility of aluminum at pressures $\geq$1 TPa. *Sov. Phys. JETP* **61**, 869–873.

Skidmore, I.C. & Morris, E. (1962). Experimental equation-of-state data for uranium and its interpretation in the critical region. In *Thermodynamics of Nuclear Materials*, pp. 173–216. Vienna: IAEA.

Syassen, K. & Holzaphel, W.B. (1978). Isothermal compression of Al and Ag to 120 kbar. *J. Appl. Phys.* **49**, 4427–4430.

Tahir, N.A., Deutsch, C., Fortov, V.E., Gryaznov, V., Hoffmann, D. H.H., Kulish, M., Lomonosov, I.V., Mintsev, V., Ni, P., Nikolaev, D., Piriz, A.R., Shilkin, N., Spiller, P., Shutov, A., Temporal, M., Ternovoi, V., Udrea, S. & Varentsov, D. (2005*a*). Proposal for the study of thermophysical properties of high-energy-density matter using current and future heavy-ion accelerator facilities at GSI Darmstadt. *Phys. Rev. Lett.* **95**, 035001-1035001-4.

Tahir, N.A., Kain, V., Schmidt, R., Shutov, A., Lomonosov, I.V., Gryaznov, V., Piriz, A.R., Temporal, M., Hoffmann, D. H.H. & Fortov, V.E. (2005*b*). The CERN large hadron collider as a tool to study high-energy density matter. *Phys. Rev. Lett.* **94**, 135004-1135004-4.

Tahir, N.A., Kim, V., Lomonosov, I.V., Grigoriev, D.A., Piriz, A.R., Weick, H., Geissel, H. & Hoffmann, D.H.H. (2007). High energy density physics problems related to liquid jet lithium target for Super--FRS fast extraction scheme. *Laser Part. Beams* **25**, 295–304.

Temporal, M., Cela, J. Lopez, J., Piriz, A.R., Grandjouan, N., Tahir, N.A. & Hoffmann, D.H.H. (2005). Compression of a cylindrical hydrogen sample driven by an intense co-axial heavy ion beam. *Laser Part. Beams* **23**, 137–142.

van Thiel, M., ed. (1977). *Compendium of Shock Wave Data. Report UCRL-50108*. Livermore: Lawrence Livermore Lab.

Toloukian, Yu.S., Kirby, R.K., Taylor, R.E. & Desay, P.D. (1975). In *Thermophysical Properties of Matter*, vol. 12, p. 2. New York: IFI/Plenum.

Trunin, R.F. (1986). Compressibility of various substances at high shock pressures. Review. *Bull. Acad. Sci. USSR* **22**, 103–106.

Trunin, R.F., Gudarenko, L.F., Zhernokletov, M.V. & Simakov, G.V. (2001). *Experimental Data on Shock Compression and Adiabatic Expansion of Condensed Matter* [in Russian]. Sarov: RFNC-VNIIEF.

Trunin, R.F., Panov, M.V. & Medvedev, A.B. (1995*a*). Compressibility of iron, aluminum, molybdenum, titanium and tantalum at shock-wave pressures of 1–2.5 TPa. *Sov. Phys. JETP Lett.* **62**, 591–594.

Trunin, R.F., Panov, M.V. & Medvedev, A.B. (1995*b*). Shock compressibilities of iron, aluminum and tantalum at terapascal pressures. *Chem. Phis.* **14**, 97–99.

Trunin, R.F., Podurets, M.A., Moiseev, B.N., Simakov, G.V. & Popov, L.V. (1969). Relative compressibility of copper, cadmium and lead at high pressures. *Sov. Phys. JETP* **29**, 630–631.

Trunin, R.F., Podurets, M.A., Moiseev, B.N.V., Simakov, G. & Sevastyanov, A.G. (1993). Determination of the shock compressibility of iron at pressures up to 10 TPa (100 Mbar). *Sov. Phys. JETP* **76**, 1095–1098.

Trunin, R.F., Podurets, M.A., Popov, L.V., Zubarev, V.N., Bakanova, A.A., Ktitorov, V.M., Sevastyanov, A.G., Simakov, G.V. & Dudoladov, I.P. (1992). Measurement of the iron compressibility at pressures of 5.5 TPa. *Sov. Phys. JETP* **75**, 777–780.

Vladimirov, A.S., Voloshin, N.P., Nogin, V.N., Petrovtsev, A.V. & Simonenko, V.A. (1984). Shock compressibility of aluminum at $p \geqslant 1$ Gbar. *Sov. Phys. JETP Lett.* **39**, 85–88.

Volkov, L.P., Voloshin, N.P., Vladimirov, A.S., Nogin, V.N. & Simonenko, V.A. (1981). Shock compressibility of aluminum at pressure 10 Mbar. *Sov. Phys. JETP Lett.* **31**, 588–591.

Voropinov, A.I., Gandelman, G.M. & Podvalnyi, V.G. (1970). Electron energy spectra and state equations of solids at high pressures and temperatures. *Sov. Phys. Usp.* **13**, 56.

Walsh, J.M., Rice, M.H., McQueen, R.G. & Yarger, F.L. (1957). Shock-wave compressions of twenty-seven metals equations of state of metals. *Phys. Rev.* **108**, 196–221.

Wang, Y., Chen, D. & Zhang, X. (2000). Calculated equation of state of Al, Cu, Ta, Mo, and W to 1000 GPa. *Phys. Rev. Lett.* **84**, 3220–3223.

Wentzcovich, R.M. & Lam, P.K. (1991). fcc-to-hcp transformation: A first-principal investigation. *Phys. Rev. B* **44**, 9155–9158.

Yoo, C.-S., Holmes, N.C., Ross, M., Webb, D.J. & Pike, C. (1993). Shock temperature and melting of iron at Earth core conditions. *Phys. Rev. Lett.* **70**, 3931–3934.

Young, D. (1977). A soft-sphere model for liquid metals. Report UCRL-52352. Livermore: Lawrence Livermore Lab.

Young, D.A. & Alder, B.J. (1971). Critical points of metals from the van der Waals model. *Phys. Rev. A* **3**, 364–371.

Young, D.A. & Corey, E.M. (1995). A new global equation of state model for hot, dense matter. *J. Appl. Phys.* **78**, 3748–3755.

Zeldovich, Y.-B. & Raizer, Y-.P. (1966). *Physics of Shock Waves and High–Temperature Hydrodynamic Phenomena*. New York: Academic Press.

Zhernokletov, M.V., Simakov, G.V., Sutulov, Yu.N. & Trunin, R.F. (1995). Unload isentrops of aluminium, iron, molybdenum, lead and tantal [in russian]. *Teplofiz. Vys. Temp.* **70**, 40–43.

Zhernokletov, M.V., Zubarev, V.N., Trunin, R.F. & Fortov, V.E. (1996). *Experimental Data on Shock Compressibility and Adiabatic Expansion of Condensed Matter at High Energy Density* [in Russian]. Chernogolovka: Inst. Chem. Phys. in Chernogolovka RAS.

APPENDIX EOS data

These tables present EOS coefficients[2] as well as calculations of isotherms and the principal shock adiabat.[3] For more details, such as units, see also section *Nomenclature*.

Table 1. *EOS coefficients*

EOS parameter	Numerical value	EOS parameter	Numerical value	EOS parameter	Numerical value
R	0.930	T_g	300		
Z	13	T_b	8	T_{sa}	6
a_1	326.35	γ_{e0}	0.7	T_{ca}	25
a_2	−1035.44	γ_m	−0.50	θ_{0s}	0.1
a_3	858.51	γ_{ei}	0.4	γ_{0s}	2.19
a_4	−160.59	σ_e	1.0	B_s	0.7
a_5	11.17	σ_d	9.99E+9	D_s	0.7
V_0	0.3690	β_0	0.0500	θ_{0l}	157
V_{0c}	0.3614	β_i	0.0242	γ_{0l}	1.78
E_{sub}	12.1	β_{m}	0.0	B_l	1.05
A_c	−12.91	σ_i	0.3	σ_{m0}	0.923
B_c	40.96	T_i	50	T_{m0}	0.933
C_c	−28.05	σ_Z	0.8	A_m	2.24
m	8.0	T_Z	200	B_m	−5.64
n	4.99	σ_a	0.14	C_m	0.21
l	0.70	T_a	30		

Table 2. T = *0 K Isotherm*

P_c, GPa	V_c, cc/g	E_c, kJ/g	c_c, km/s
4.292E−05	3.620E−01	0.000E+00	5.432E+00
1.723E+01	3.105E−01	3.889E−01	6.776E+00
4.722E+01	2.663E−01	1.738E+00	8.157E+00
9.657E+01	2.284E−01	4.365E+00	9.599E+00
1.748E+02	1.959E−01	8.649E+00	1.112E+01
2.955E+02	1.680E−01	1.504E+01	1.272E+01
4.780E+02	1.441E−01	2.409E+01	1.442E+01
7.490E+02	1.236E−01	3.642E+01	1.622E+01
1.146E+03	1.060E−01	5.278E+01	1.814E+01
1.722E+03	9.093E−02	7.405E+01	2.017E+01
2.548E+03	7.799E−02	1.012E+02	2.233E+01
3.723E+03	6.689E−02	1.355E+02	2.461E+01
5.380E+03	5.737E−02	1.781E+02	2.703E+01
7.702E+03	4.921E−02	2.308E+02	2.958E+01
1.093E+04	4.221E−02	2.951E+02	3.228E+01
1.541E+04	3.620E−02	3.732E+02	3.512E+01
2.156E+04	3.105E−02	4.672E+02	3.811E+01
2.999E+04	2.663E−02	5.796E+02	4.125E+01
4.148E+04	2.284E−02	7.134E+02	4.453E+01
5.705E+04	1.959E−02	8.716E+02	4.798E+01

[2] units of coefficients in this table correspond to initial units in the EOS, *E*equals;1 kJ/g, V=1 cm^3/g, T=1000 K, so that, for example $\beta_0=E/T^2=10_{-3}$ J/(gK^2) and so on.

[3] here in tables record 1.234E+05 means $1.234\times10^{+05}$

https://doi.org/10.1017/S0263034607000687 Published online by Cambridge University Press

7.806E+04	1.680E−02	1.058E+03	5.157E+01
1.063E+05	1.441E−02	1.276E+03	5.532E+01
1.442E+05	1.236E−02	1.530E+03	5.924E+01
1.946E+05	1.060E−02	1.824E+03	6.331E+01
2.618E+05	9.093E−03	2.165E+03	6.757E+01
3.508E+05	7.799E−03	2.557E+03	7.201E+01
4.685E+05	6.689E−03	3.007E+03	7.667E+01
6.240E+05	5.737E−03	3.522E+03	8.158E+01
8.292E+05	4.921E−03	4.109E+03	8.679E+01
1.100E+06	4.221E−03	4.778E+03	9.239E+01
1.459E+06	3.620E−03	5.538E+03	9.849E+01

Table 3. T = *293 K Isotherm*

P, GPa	*V*, cc/g	*E*, kJ/g	*H*, kJ/g	c_T, km/s	c_S, km/s
2.916E+03	7.380E−02	1.121E+02	3.273E+02	2.310E+01	2.310E+01
2.592E+03	7.738E−02	1.023E+02	3.028E+02	2.240E+01	2.241E+01
2.301E+03	8.113E−02	9.315E+01	2.798E+02	2.172E+01	2.173E+01
2.040E+03	8.506E−02	8.464E+01	2.581E+02	2.106E+01	2.106E+01
1.806E+03	8.918E−02	7.674E+01	2.378E+02	2.040E+01	2.041E+01
1.597E+03	9.351E−02	6.941E+01	2.187E+02	1.976E+01	1.977E+01
1.410E+03	9.804E−02	6.261E+01	2.009E+02	1.913E+01	1.913E+01
1.243E+03	1.028E−01	5.633E+01	1.841E+02	1.851E+01	1.851E+01
1.094E+03	1.078E−01	5.053E+01	1.684E+02	1.790E+01	1.791E+01
9.611E+02	1.130E−01	4.519E+01	1.538E+02	1.730E+01	1.731E+01
8.427E+02	1.185E−01	4.027E+01	1.401E+02	1.671E+01	1.672E+01
7.374E+02	1.242E−01	3.575E+01	1.274E+02	1.614E+01	1.615E+01
6.438E+02	1.302E−01	3.161E+01	1.155E+02	1.557E+01	1.558E+01
5.608E+02	1.366E−01	2.783E+01	1.044E+02	1.502E+01	1.503E+01
4.872E+02	1.432E−01	2.439E+01	9.414E+01	1.447E+01	1.448E+01
4.220E+02	1.501E−01	2.125E+01	8.461E+01	1.393E+01	1.395E+01
3.645E+02	1.574E−01	1.841E+01	7.577E+01	1.341E+01	1.342E+01
3.137E+02	1.650E−01	1.584E+01	6.760E+01	1.289E+01	1.291E+01
2.689E+02	1.730E−01	1.353E+01	6.006E+01	1.238E+01	1.240E+01
2.295E+02	1.814E−01	1.146E+01	5.310E+01	1.189E+01	1.190E+01
1.950E+02	1.902E−01	9.619E+00	4.670E+01	1.140E+01	1.142E+01
1.647E+02	1.994E−01	7.982E+00	4.083E+01	1.092E+01	1.094E+01
1.383E+02	2.091E−01	6.539E+00	3.545E+01	1.044E+01	1.047E+01
1.152E+02	2.192E−01	5.276E+00	3.053E+01	9.977E+00	1.000E+01
9.514E+01	2.299E−01	4.180E+00	2.605E+01	9.520E+00	9.550E+00
7.776E+01	2.410E−01	3.239E+00	2.198E+01	9.069E+00	9.103E+00
6.274E+01	2.527E−01	2.441E+00	1.829E+01	8.625E+00	8.663E+00
4.980E+01	2.649E−01	1.775E+00	1.497E+01	8.187E+00	8.231E+00
3.870E+01	2.778E−01	1.231E+00	1.198E+01	7.755E+00	7.806E+00
2.923E+01	2.912E−01	7.980E−01	9.311E+00	7.329E+00	7.387E+00
2.118E+01	3.053E−01	4.675E−01	6.935E+00	6.908E+00	6.975E+00
1.438E+01	3.201E−01	2.305E−01	4.835E+00	6.491E+00	6.568E+00
8.674E+00	3.357E−01	7.877E−02	2.990E+00	6.077E+00	6.168E+00
3.921E+00	3.519E−01	4.372E−03	1.384E+00	5.666E+00	5.772E+00
1.007E−04	3.690E−01	−1.105E−08	3.716E−05	5.246E+00	5.369E+00

https://doi.org/10.1017/S0263034607000687 Published online by Cambridge University Press

Table 4. *Principal Hugoniot (here* T *is in 1000 K)*

P, GPa	T, 1000 k	V, cc/g	S, J/(gk)	E, kJ/g	U_S, km/s	u_P, km/s
1.000E−04	2.930E−01	3.690E−01	3.576E−07	1.158E−07	0.000E+00	0.000E+00
2.500E+00	3.130E−01	3.581E−01	1.137E−03	1.358E−02	5.592E+00	1.650E−01
3.000E+00	3.170E−01	3.561E−01	1.940E−03	1.930E−02	5.633E+00	1.965E−01
4.000E+00	3.251E−01	3.523E−01	4.333E−03	3.339E−02	5.715E+00	2.583E−01
5.000E+00	3.333E−01	3.487E−01	7.733E−03	5.070E−02	5.794E+00	3.185E−01
6.000E+00	3.420E−01	3.453E−01	1.255E−02	7.113E−02	5.871E+00	3.771E−01
8.000E+00	3.604E−01	3.389E−01	2.602E−02	1.202E−01	6.020E+00	4.903E−01
1.000E+01	3.807E−01	3.332E−01	4.490E−02	1.792E−01	6.164E+00	5.987E−01
1.500E+01	4.413E−01	3.207E−01	1.133E−01	3.626E−01	6.500E+00	8.515E−01
2.000E+01	5.174E−01	3.103E−01	2.046E−01	5.871E−01	6.811E+00	1.084E+00
2.500E+01	6.096E−01	3.015E−01	3.097E−01	8.441E−01	7.100E+00	1.299E+00
3.000E+01	7.177E−01	2.938E−01	4.212E−01	1.127E+00	7.372E+00	1.502E+00
4.000E+01	9.790E−01	2.812E−01	6.445E−01	1.757E+00	7.875E+00	1.874E+00
5.000E+01	1.295E+00	2.710E−01	8.540E−01	2.451E+00	8.334E+00	2.214E+00
6.000E+01	1.660E+00	2.625E−01	1.044E+00	3.195E+00	8.758E+00	2.528E+00
8.000E+01	2.511E+00	2.491E−01	1.369E+00	4.798E+00	9.530E+00	3.098E+00
1.000E+02	3.496E+00	2.387E−01	1.634E+00	6.516E+00	1.022E+01	3.610E+00
1.126E+02	4.174E+00	2.332E−01	1.778E+00	7.646E+00	1.063E+01	3.910E+00
1.500E+02	4.691E+00	2.206E−01	2.191E+00	1.113E+01	1.173E+01	4.719E+00
1.779E+02	5.015E+00	2.128E−01	2.498E+00	1.390E+01	1.245E+01	5.272E+00
2.000E+02	6.112E+00	2.070E−01	2.715E+00	1.620E+01	1.296E+01	5.693E+00
2.500E+02	8.769E+00	1.960E−01	3.118E+00	2.163E+01	1.403E+01	6.577E+00
3.000E+02	1.167E+01	1.873E−01	3.438E+00	2.726E+01	1.499E+01	7.384E+00
4.000E+02	1.819E+01	1.742E−01	3.926E+00	3.896E+01	1.672E+01	8.827E+00
5.000E+02	2.561E+01	1.648E−01	4.289E+00	5.106E+01	1.826E+01	1.011E+01
6.000E+02	3.370E+01	1.576E−01	4.575E+00	6.343E+01	1.966E+01	1.126E+01
8.000E+02	5.061E+01	1.470E−01	5.008E+00	8.882E+01	2.215E+01	1.333E+01
1.000E+03	6.706E+01	1.391E−01	5.334E+00	1.150E+02	2.434E+01	1.516E+01
1.500E+03	1.036E+02	1.255E−01	5.935E+00	1.827E+02	2.896E+01	1.911E+01
2.000E+03	1.349E+02	1.164E−01	6.391E+00	2.526E+02	3.284E+01	2.248E+01
2.500E+03	1.632E+02	1.100E−01	6.772E+00	3.238E+02	3.625E+01	2.545E+01
3.000E+03	1.895E+02	1.052E−01	7.106E+00	3.957E+02	3.935E+01	2.813E+01
4.000E+03	2.390E+02	9.873E−02	7.679E+00	5.406E+02	4.489E+01	3.288E+01
5.000E+03	2.862E+02	9.481E−02	8.165E+00	6.855E+02	4.983E+01	3.703E+01
6.000E+03	3.327E+02	9.252E−02	8.590E+00	8.295E+02	5.436E+01	4.073E+01
8.000E+03	4.249E+02	9.102E−02	9.313E+00	1.112E+03	6.260E+01	4.716E+01
1.000E+04	5.158E+02	9.182E−02	9.913E+00	1.386E+03	7.009E+01	5.265E+01

https://doi.org/10.1017/S0263034607000687 Published online by Cambridge University Press